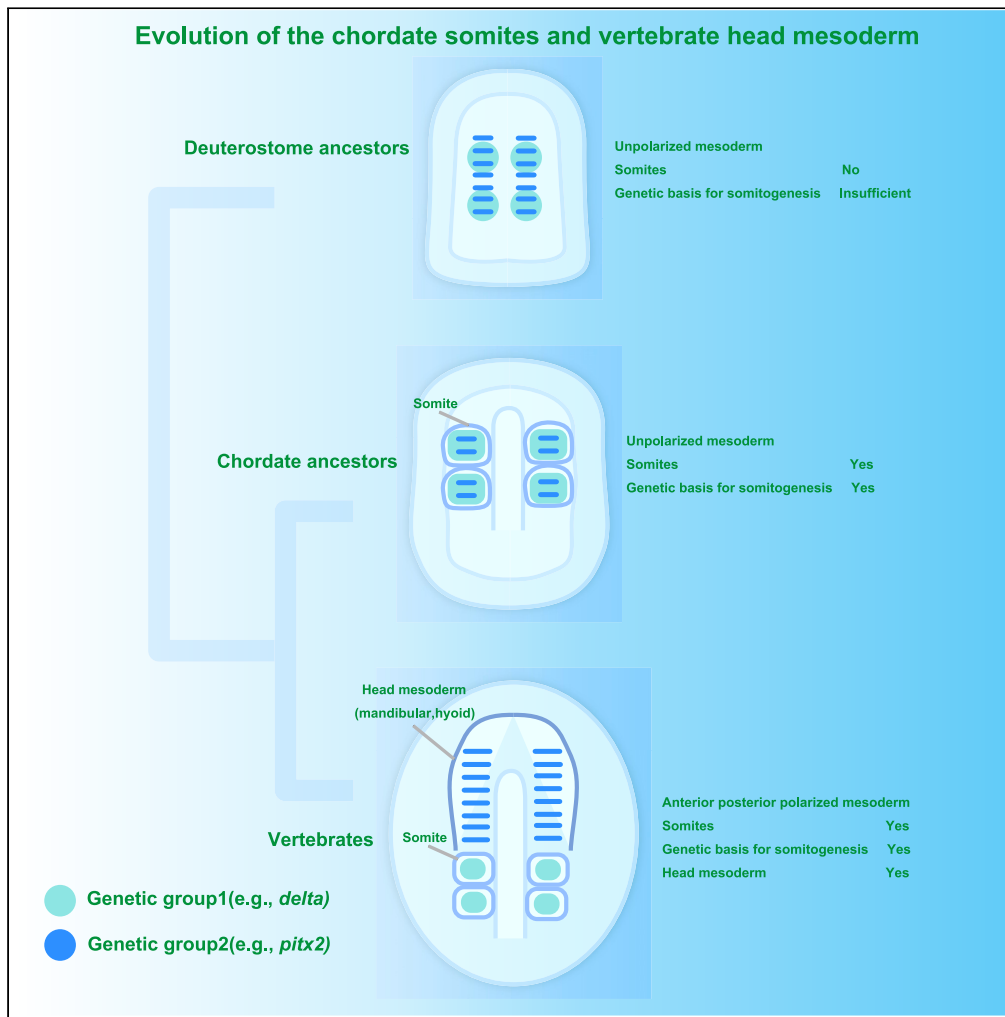


Article

# Ultrastructure of the lamprey head mesoderm reveals evolution of the vertebrate head



Takayuki Onai,  
Noritaka Adachi,  
Hidetoshi  
Urakubo, Fumiaki  
Sugahara,  
Toshihiro Aramaki,  
Mami Matsumoto,  
Nobuhiko Ohno

tonai@u-fukui.ac.jp

**Highlights**

Rosette pattern seen in somites is not a primal identity of segmentation

The vertebrate head mesoderm diverged during the early phase of evolution

Rostro-caudal segregation of mesodermal genes enabled to evolve the head mesoderm

Somites arose from an ancient deuterostome endomesoderm during gastrulation

Onai et al., iScience 26, 108338  
December 15, 2023 © 2023 The Authors.  
<https://doi.org/10.1016/j.isci.2023.108338>



## Article

## Ultrastructure of the lamprey head mesoderm reveals evolution of the vertebrate head

Takayuki Onai,<sup>1,2,13,\*</sup> Noritaka Adachi,<sup>3,11</sup> Hidetoshi Urakubo,<sup>4,12</sup> Fumiaki Sugahara,<sup>5</sup> Toshihiro Aramaki,<sup>6</sup> Mami Matsumoto,<sup>7,8</sup> and Nobuhiko Ohno<sup>9,10</sup>

## SUMMARY

The cranial muscle is a critical component in the vertebrate head for a predatory lifestyle. However, its evolutionary origin and possible segmental nature during embryogenesis have been controversial. In jawed vertebrates, the presence of pre-otic segments similar to trunk somites has been claimed based on developmental observations. However, evaluating such arguments has been hampered by the paucity of research on jawless vertebrates. Here, we discovered different cellular arrangements in the head mesoderm in lamprey embryos (*Lethenteron camtschaticum*) using serial block-face scanning electron and laser scanning microscopies. These cell populations were morphologically and molecularly different from somites. Furthermore, genetic comparison among deuterostomes revealed that mesodermal gene expression domains were segregated antero-posteriorly in vertebrates, whereas such segregation was not recognized in invertebrate deuterostome embryos. These findings indicate that the vertebrate head mesoderm evolved from the anteroposterior repatterning of an ancient mesoderm and developmentally diversified before the split of jawless and jawed vertebrates.

## INTRODUCTION

After Goethe proposed in the 18<sup>th</sup> century that skulls were derived from trunk vertebrae,<sup>1</sup> the vertebrate head has been considered to have evolved from the modification of trunk segmental elements such as vertebrae and somites (a view of segmentalists).<sup>2–4</sup> Contrary to Goethe's idea, the vertebrate head is assumed to have evolved as a new unsegmented head (a view of non-segmentalists).<sup>5,6</sup> To date, no definite solution to this debate has been obtained,<sup>7</sup> and the main controversy centers on the origin of the pre-otic head mesoderm.<sup>2,5,7</sup> Three pairs of head cavities, which have been repeatedly regarded as serial homologs of trunk somites, develop during embryogenesis in elasmobranchs and lampreys (Figures 1A–1C and S1B)<sup>8,9</sup> and have been proposed as homologs of rostral somites in the cephalochordate amphioxus (Figure S1A).<sup>10,11</sup> Furthermore, vestiges of somites, known as somitomeres, have been discovered in the head mesoderm of early chicken embryos<sup>12</sup> before the formation of the head cavity (Figure S1C).<sup>5</sup> Somitomeres were also found in the teleost (*Oryzias latipes*), Chondrichthyes (*Squalus acanthias*), and mouse embryos.<sup>13–15</sup> However, replication studies of somitomeres did not detect such morphological structures, nor did gene expression profiles of head mesoderm fit well with somitomere patterns.<sup>16–19</sup> Although the presence of such segmental features of the head has been denied by some researchers,<sup>20–22</sup> there have been insufficient molecular and morphological studies to resolve this dichotomy.<sup>10,19,23–28</sup>

Extant cyclostomes (lampreys and hagfish) share several traits with fossil jawless vertebrates, making them useful for understanding the origin of vertebrates.<sup>29–31</sup> Moreover, conflicts on the origin of the vertebrate head have been unsettled partly due to the poor understanding of the lamprey head mesoderm.<sup>2,7</sup> On the early vertebrate evolution, there has been two major hypotheses about the position of lampreys and hagfishes, craniate, and cyclostome hypotheses.<sup>29</sup> Based on morphological data, lampreys are considered to be a closer relative to gnathostomes than to hagfishes, and hagfishes are regarded to retain primitive traits in the craniate hypothesis.<sup>32</sup> On the other hand, the cyclostome hypothesis supported by molecular data indicates that hagfishes are anatomically derived lineage.<sup>33</sup>

<sup>1</sup>Department of Anatomy, University of Fukui, School of Medical Sciences, 23-3, Matsuokashimoaizuki, Eiheiji, Yoshida, Fukui, Japan

<sup>2</sup>Life Science Innovation Center, University of Fukui, 23-3, Matsuokashimoaizuki, Eiheiji, Yoshida, Fukui, Japan

<sup>3</sup>Aix-Marseille Université, IBDM, CNRS UMR 7288, Campus De Luminy Case 907, 13288 Marseille Cedex 9, France

<sup>4</sup>Section of Electron Microscopy, National Institute for Physiological Sciences, 38, Nishigonaka, Myodaiji, Okazaki, Aichi, Japan

<sup>5</sup>Division of Biology, Hyogo Medical University, 1-1, Mukogawa, Nishinomiya, Hyogo, Japan

<sup>6</sup>Graduate School of Frontier Biosciences, Osaka University, 1-1, Yamadaoka, Suita, Osaka, Japan

<sup>7</sup>Section of Electron Microscopy, Supportive Center for Brain Research, National Institute for Physiological Sciences, 38, Nishigonaka, Myodaiji, Okazaki, Aichi, Japan

<sup>8</sup>Department of Developmental and Regenerative Biology, Nagoya City University Graduate School of Medical Sciences, 1, Kawasumi, Mizuho, Nagoya, Aichi, Japan

<sup>9</sup>Department of Anatomy, Division of Histology and Cell Biology, School of Medicine, Jichi Medical University, 3311-1, Yakushiji, Shimotsuke, Tochigi, Japan

<sup>10</sup>Division of Ultrastructural Research, National Institute for Physiological Sciences, 38, Nishigonaka, Myodaiji, Okazaki, Aichi, Japan

<sup>11</sup>Present address: Tokyo Medical and Dental University, 1-5-45, Yushima, Bunkyo, Tokyo, Japan

<sup>12</sup>Present address: Fujita Health University, 1-98 Dengakugakubo, Kutsukake-cho, Toyoake, Aichi, Japan

<sup>13</sup>Lead contact

\*Correspondence: tonai@u-fukui.ac.jp

<https://doi.org/10.1016/j.isci.2023.108338>



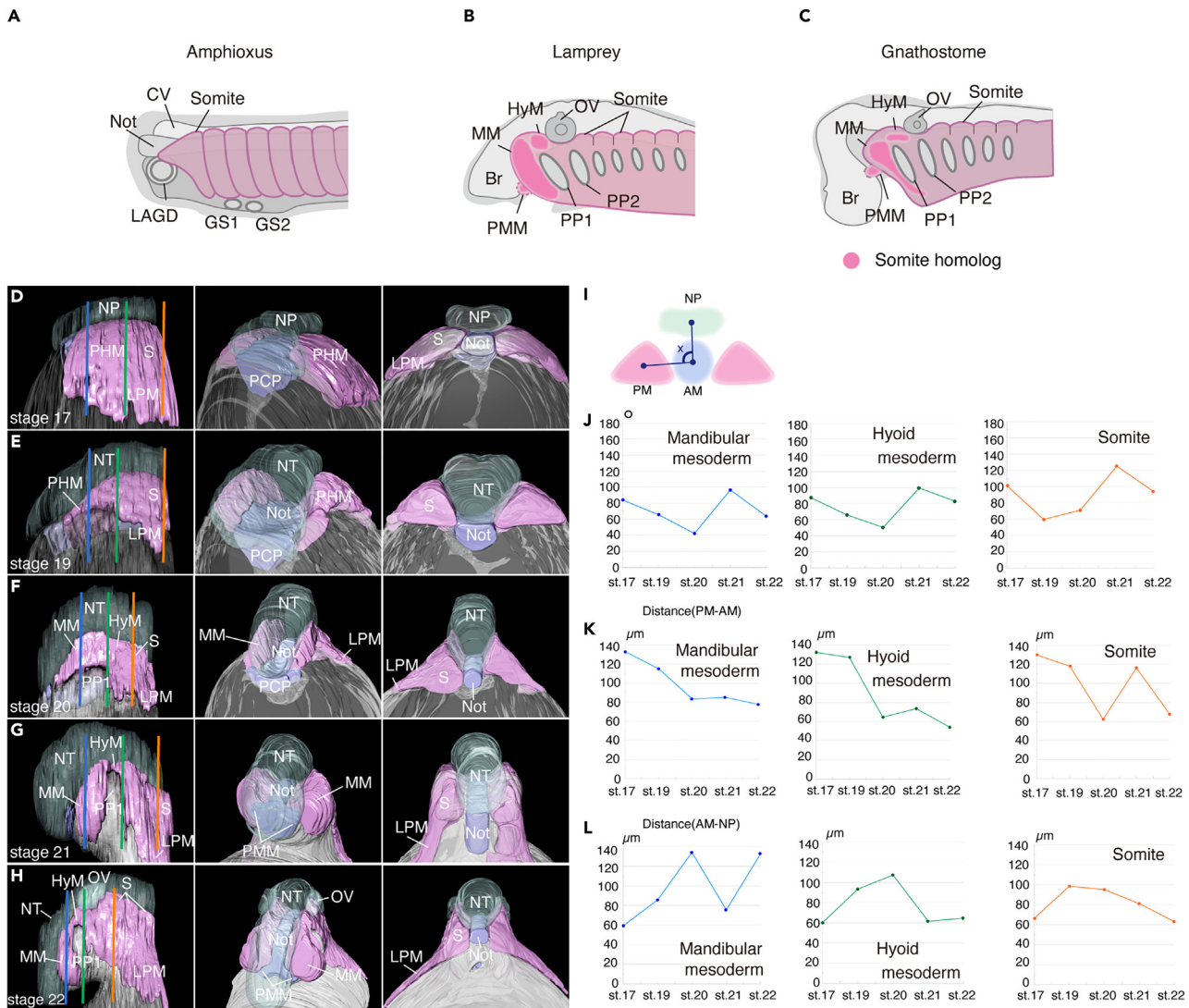


**Figure 1. Formation of the head/trunk mesoderm in lamprey (*Lethenteron camtschaticum*) embryos**

See also [Figure S1](#).

(A–C) Comparison of the chordate heads. Somites are located at the rostral end of the amphioxus (A), and three pairs of somite homologs have been suggested in the head mesoderm of lampreys (B) and gnathostomes (C).

(D–H) 3D reconstruction of lamprey embryos. The blue (mandibular mesoderm), green (hyoid mesoderm), and orange (somites) lines in the left panels correspond to the optical sections analyzed in (J–L). The left panels are side views anterior to the left; the center panels are left anterior oblique views, and the right panels are posterior views.

(I–L) Quantitative analysis of lamprey morphology in terms of mandibular mesoderm (blue), hyoid mesoderm (green), and somites (orange). (I) Scheme of the inner product (x) calculation of the paraxial mesoderm, axial mesoderm, and neural plate. (J–L) Time sequences of the inner products (J), distance between the paraxial and axial mesoderm (K), and the distance between the axial mesoderm and neural plate (tube) (L). AM, axial mesoderm; Br, brain; CV, cerebral vesicle; GS, gill slit; HyM, hyoid mesoderm; LAGD, left anterior gut diverticulum; LPM, lateral plate mesoderm; MM, mandibular mesoderm; Not, notochord; NP, neural plate; NT, neural tube; OV, otic vesicle; PCP, pre-chordal plate; PHM, paraxial head mesoderm; PM, paraxial mesoderm; PMM, premandibular mesoderm; PP, pharyngeal pouch; S, somite.

Recent fossil study on hagfishes from the Cretaceous Tethys sea, as well as a comparative developmental study on lampreys, hagfishes, and gnathostomes also strength the cyclostome hypothesis.<sup>34,35</sup> Hagfishes are marine fishes living in deep sea, and the developmental sequences of the head mesoderm seem to be highly modified because of the degenerated eyes and the loss of extraocular muscles.<sup>36,37</sup> Therefore, it is considered that they experienced long selective time which related to evolve highly derived characters.<sup>33</sup> On the other hand, lampreys possess eyes and extraocular muscles and are more likely to retain their ancestral condition of the head mesoderm.<sup>9</sup>

In 1902, Koltzoff observed head somites of lamprey embryos in paraffin sections, but the tissues tended to peel off during sectioning because of a large number of yolk granules, and the acidic fixative distorted the embryonic morphology.<sup>9,38,39</sup> Subsequent studies on the lamprey head mesoderm were insufficient to determine whether it contains somites.<sup>39,40</sup> Therefore, we reinvestigated the formation of the head mesoderm and trunk somites in lamprey embryos using confocal laser scanning microscopy, which prevents tissue destruction by yolk granules, and examined the tissue ultrastructures using transmission electron microscopy (TEM), which is useful for detecting tiny cavities. Furthermore, we performed serial block-face scanning electron microscopy (SBF-SEM) to reconstruct and compare cellular morphology and arrangements between somites and the head mesoderm, especially the mandibular and hyoid mesoderm, located in anatomically comparable positions in the embryo. To understand the evolutionary history of the somites and head mesoderm in the deuterostome phylogeny, we also analyzed morphology and gene expression patterns of cephalochordate (*Branchiostoma floridae*), which is the most basal living chordate, and hemichordate (*Ptychodera flava*), which is a member of ambulacraria phyla, one of the two superphyla in deuterostomes.

## RESULTS

### Rosette-shaped somites

Somites become evident at the rostral end of the presomitic mesoderm in vertebrates.<sup>41</sup> One of the important characteristics of somites is their “rosette” shape (radial epithelial cells surrounding a central cavity).<sup>42</sup> Each somite was situated in a row along the A/P axis separated by an acellular fissure (Figures S1F–S1H).<sup>43</sup> Unlike previous observations, the central cavity of the rosette in the somites was tiny in lampreys (Figure S1F)<sup>9</sup> but evident in gnathostomes, which contain somitocoel cells that form vertebral joints and intervertebral disks (Figure S1G).<sup>44</sup> In cephalochordates, somites were formed via the rearrangement of cells near the neurenteric canal, except for rostral somites that arise from the dorsal wall of the gut (Figures S1E and S1H).<sup>45</sup> Somites, a synapomorphy of chordates, were not formed in tornaria larvae of the hemichordate *Ptychodera flava* (Figures S1D and S1H).<sup>7</sup>

### Morphospecialization of the head mesoderm

To quantitatively understand the developmental dynamics of the head mesoderm, we first performed a three-dimensional (3D) reconstruction of the paraxial mesoderm in lamprey embryos. At Tahara stage 17 (5 days post-fertilization),<sup>46</sup> the dorsal mesoderm was a gentle sheet beneath the neural plate (Figure 1D), the paraxial mesoderm represented a triangle, and the axial mesoderm projected inward to form a valley at stage 19 (Figure 1E). At stage 20, the mandibular mesoderm grew dorsally, and pharyngeal pouch 1 (PP1) was located beneath it (Figure 1F). The hyoid mesoderm was located on the expanded PP1 by stage 21, and the mandibular mesoderm shifted from the dorsal to the ventral side, forming the mandibular arch mesoderm anterior to PP1 (Figure 1G). At stage 22, the otic vesicles became visible (Figure 1H).

Quantitative analysis showed that the inner product (angle) between the paraxial, axial mesoderm, and neural plate (tube) decreased until stage 20 in the head mesoderm and until stage 19 in the somites and then started to increase again (Figures 1I and 1J). Time-series changes in the distance between the paraxial and axial mesoderm were similar for the mandibular and hyoid mesoderm (Figure 1K). Similarly, the distance between the axial mesoderm and neural tube increased until stage 20 and then decreased at stage 21 when the premandibular mesoderm elongated laterally at the mandibular and hyoid mesoderm but only increased until stage 19 in the somites (Figure 1L). Thus, the paraxial mesoderm experiences dynamic morphological changes that lead to the specialization of each region.

### Distinct cell clusters in the head mesoderm

Somites of lamprey embryos exhibit rosette patterns at stage 20.<sup>9</sup> Unlike somites, the head mesoderm did not include rosettes at stage 20 (Figures 2A–2C). We further examined the cell arrangements in the head mesoderm during the early pharyngeal stages. Confocal microscopy revealed that the mandibular arch mesoderm contained a small cavity surrounded by radially located cells similar to the trunk somite (Figures 2D and 2E); with cell cluster 2 medial to this, both cell cluster 1 and 2 were rosette-like (Figures 2E and 2F). Koltzoff found one large somite in the mandibular arch mesoderm.<sup>9</sup> Another rosette-like pattern was observed in the hyoid mesoderm (Figure 2G), which has a much smaller cavity than the hyoid somite found by Koltzoff.<sup>9</sup> These cell clusters began to form in the earlier stages (Figures S2A–S2I). Whether these cell clusters are the rosettes seen in somites is unclear from these results because the resolutions of cell arrangements at the 3D level were insufficient. Therefore, ultrastructural experiments were performed.

SBF-SEM analysis revealed that these cell clusters had different cell arrangements compared with somite rosettes (Figures 2H–2K and 2P–2W, Videos S1, S2, S3, S4, S5, S6, S7, and S8). Mandibular cell cluster 1 contained rostral amorphous cells and columnar cells forming a caudal line (Figures 2I, 2M, and 2Q). Mandibular cell cluster 2 consisted of amorphous and columnar cells (Figures 2J, 2N, and 2R). The hyoid cell cluster was organized into amorphous cells (Figures 2K, 2O, and 2S). Unlike somites, these cell clusters contained many acellular spaces (Figures 2L–2O). These cell clusters did not form acellular fissures seen in somites or line up as a row along the A/P axis, indicating that the head mesoderm did not contain segments at this stage (Figure 2).

At the molecular level, the absence of somitogenesis-related genes (e.g., *Notch*, *Wnt*, retinoic acid, and fibroblast growth factor signaling components) expression in the head mesoderm has previously been reported in gnathostomes.<sup>19</sup> However, no such data are available for lampreys. Using gene expression analysis, we found that the lamprey head mesoderm did not exhibit segmental expression patterns of somitogenesis-related genes (Figures S3, S6A, S6D, and S6E), indicating that cell clusters in the head mesoderm are genetically distinct from somites.

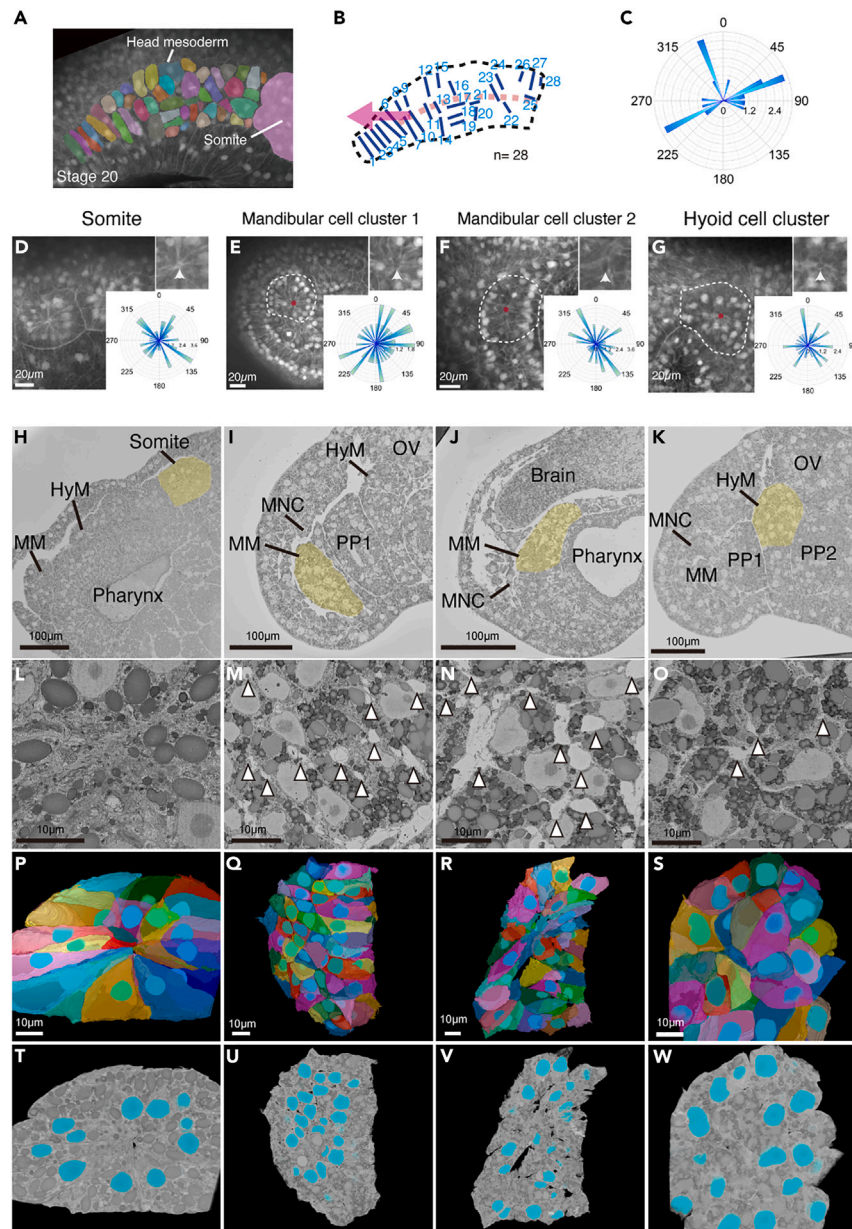


**Figure 2. Different cell clusters in the lamprey head mesoderm**

See also [Figures S2](#) and [S3](#).

(A and B) Segmentation of cells in the head mesoderm.

(C) Rose diagram of the quantified orientation of the cells in (B). Orientation is defined as the direction of a large area of cytoplasmic spread.

(D–G) Confocal laser scanning sections of trunk somites in stage 20 and cell clusters in stage 22–22.5 embryos. The bottom right panels show rose diagrams. The small photographs on the right are focused on the centers of the cell clusters (arrows). The white dotted circle encloses the cell cluster, and the red spot indicates the center of a cell cluster.  $n = 10/10$  (D),  $7/9$  (E),  $11/11$  (F),  $10/11$  (G).

(H–W) SBF-SEM of the head mesoderm cell clusters and somite. (H–K) SEM images. Yellow: analyzed regions in SBF-SEM. (L–O) Zoomed SEM images of somite (L), mandibular cell cluster 1 (M), mandibular cell cluster 2 (N), and hyoid cell cluster (O). White arrowheads indicate spaces between cells. (P–S) 3D reconstruction of somite (P, T), mandibular cell cluster 1 (Q, U), mandibular cell cluster 2 (R, V), and hyoid cell cluster (S, W). (P–S) Single-cell level 3D reconstruction. (T–W) 3D reconstruction was created by overlaying SEM section images. Nuclei (cyan). HyM, hyoid mesoderm; MM, mandibular mesoderm; MNC, mandibular neural crest; OV, otic vesicle; PP, pharyngeal pouch.

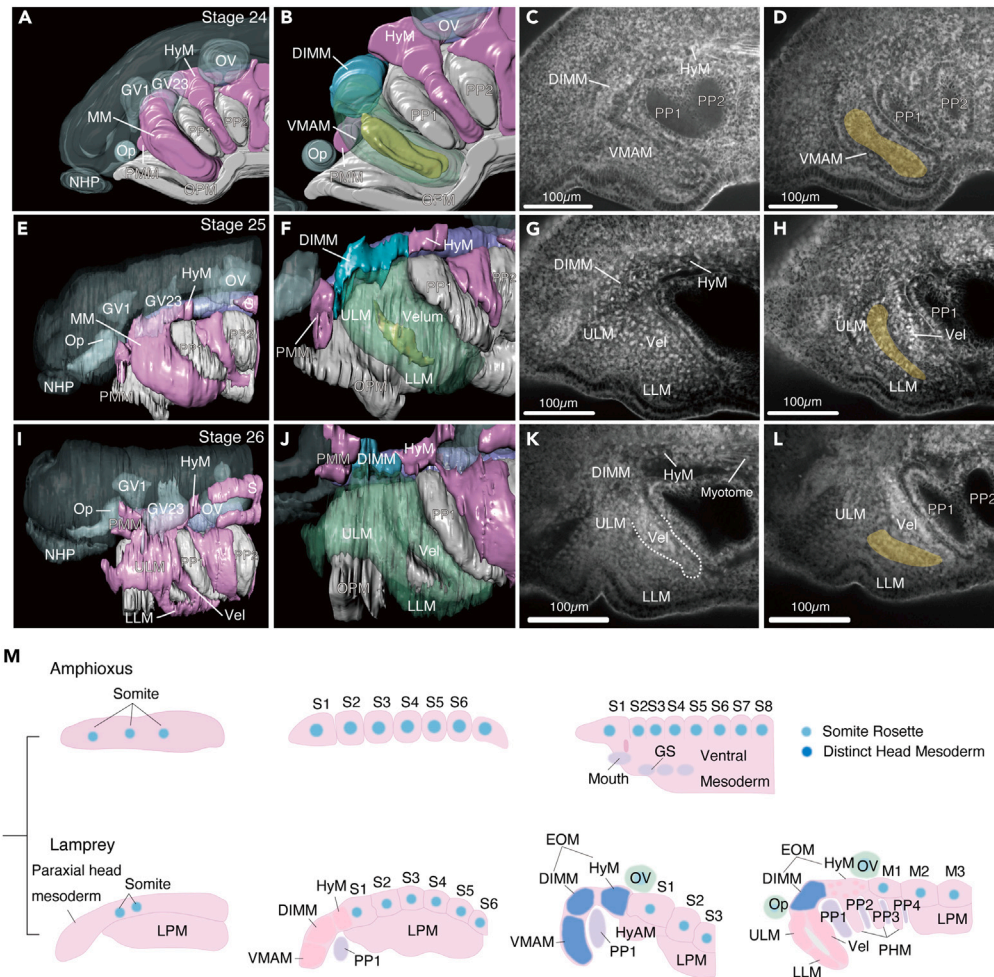


**Figure 3. Dynamics of head mesoderm cell clusters during individualization of the head muscles**

See also [Figures S4](#) and [S5](#).

(A–L) 3D reconstructions and laser scanning images of stage 24 (A–D), 25 (E–H), and 26 (I–L) lamprey embryos. The area enclosed by the white dotted line in (K) indicates velum mesoderm. Pink, mesoderm; light blue, dorsal inner mandibular mesoderm; green, ventral mandibular arch mesoderm; yellow, cavity in the mandibular mesoderm. Images show sagittal views.

(M) Comparison of rosettes and head mesoderm cell clusters in lamprey and amphioxus embryos. Right blue, somite rosette; blue, distinct head mesodermal cell clusters. DIMM, dorsal inner mandibular mesoderm; EOM, extraocular muscle; GS, gill slit; GV, ganglion trigeminal; HyAM, hyoid arch mesoderm; HyM, hyoid mesoderm; LLM, lower lip mesoderm; LPM, lateral plate mesoderm; MM, mandibular mesoderm; NHP, nasohypophyseal plate; Op, optic vesicle; OPM, oropharyngeal membrane; OV, otic vesicle; PHM, pharyngeal mesoderm; PMM, premandibular mesoderm; PP, pharyngeal pouch; S, somite; ULM, upper lip mesoderm; Vel, velum; VMAM, ventral mandibular arch mesoderm.

### Later developmental dynamism of head muscle formation

Next, we examined the later development of regions where head mesoderm cell clusters were observed. At stage 24, a cell mass was present in the dorsal inner mandibular mesoderm (DIMM) ([Figures 3A–3C](#)), where cell cluster 2 formed and was considered to differentiate into extraocular muscle (EOM).<sup>9</sup> Caudal to the DIMM, the hyoid mesoderm no longer contained the cell cluster ([Figure 3C](#)). In contrast, the ventral mandibular arch mesoderm (VMAM), where cell cluster 1 was observed, contained a long cavity ([Figures 3B](#) and [3D](#)), which separated the arch mesoderm into two rostro-caudal cell populations.

At stage 25, the premandibular mesoderm moved close to the optic vesicles ([Figures 3E](#) and [3F](#)), whereas the VMAM exhibited swelling of the upper and lower lips and velum mesoderm ([Figures 3F–3H](#)). TEM analysis showed that cells in the hyoid mesoderm were separated ([Figures 3G](#), [S4Ci](#), and [S4Cii](#)), whereas those in the premandibular and mandibular mesoderms were closely located ([Figures S4Ai](#) and [S4Bii](#)). Cell junctions connected cells in the VMAM, and the cavity in the VMAM was opened to the pharynx and contained individual cells ([Figures S4Di–S4Div](#)).

At stage 26, the cavity in the VMAM opens laterally ([Figures 3I](#), [3J](#), and [3L](#)). The extensive rostral growth of the lip mesoderm indicates that individualization of the oral cavity proceeds rapidly. Dorsally, the retinal progenitors made contact with the premandibular mesoderm,

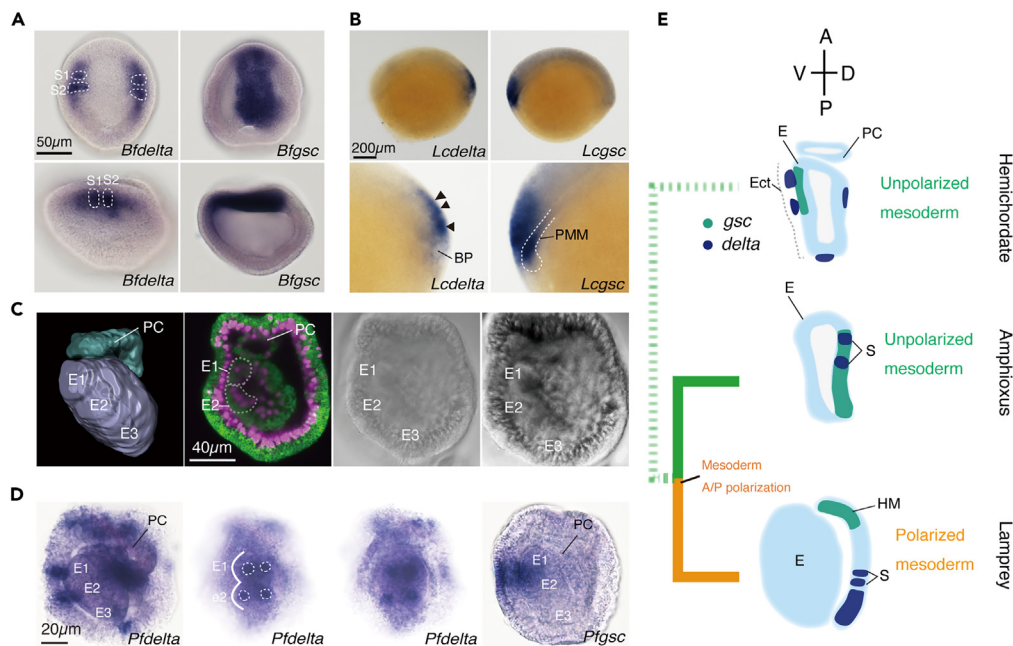


**Figure 4. A/P mesodermal repatterning evolved for the emergence of the vertebrate head mesoderm**

See also Figures S6–S8.

(A) Expression patterns of *delta* (n = 16) and *gsc* (n = 12) in amphioxus late gastrula embryos.

(B) *Delta* (n = 3) and *gsc* (n = 3) expression in lamprey stage 20 embryos. Arrow heads indicate expression domains of *delta*. (C) From left to right: 3D reconstruction of *Ptychodera flava* late gastrula embryo. Purple; endomesoderm; green, protocoele cells. E1–E3 indicate regions in the endomesoderm. Laser scanning section. Green, CellMask Deep Red; magenta, DAPI. Bright-field view. 3D view of the bright field.

(D) *Delta* (n = 18) and *gsc* (n = 5) expression in *P. flava*. White dotted circles enclosing *delta* expression.

(E) Phylogenetic relationship of mesodermal genes in deuterostomes. A, anterior; BP, blast pore; D, dorsal; E, endomesoderm; Ect, ectoderm; HM, head mesoderm; P, posterior; PC, protocoele mesoderm; PMM, premandibular head mesoderm; S, somite; V, ventral.

suggesting that individualization of the visual system also occurred (Figures 3I and S4Ei–S4Eii). TEM analysis showed that the premandibular and mandibular mesoderm contained closely situated amorphous cells (Figures S4Ei–S4Eiv). Cells in the hyoid mesoderm were enclosed by a rich collagen-like extracellular matrix (Figures 3K and S4Ev–S4Evi). Presumptive EOMs express *pitxA*, a dorsal head mesodermal gene<sup>47</sup> (Figure S5B), whereas VMAM expressed *gsc* (Figure S5A). These findings suggested that the lamprey head mesoderm had three distinct cell clusters (Figure 3M). The mandibular arch mesoderm formation is particularly dynamic, with the mesoderm in the dorsal region turning vertically and shifting to the ventral side. These developmental sequences differ from those of rostral somites in amphioxus (Figure 3M), raising the question of whether developmental sequences of the vertebrate head mesoderm were present in the common ancestor of chordates.

### Somites arose from the ancient gut

To address this question, we compared mesodermal gene expression in *Ptychodera flava* and chordates. *Gsc* and *delta* expressions overlap in the dorsal mesoderm of amphioxus and vertebrates<sup>28</sup> but become segregated during the formation of the head/trunk mesoderm only in vertebrates (Figures 4A and 4B).<sup>28</sup> In *P. flava*, the endomesoderm was divided into three distinct regions at the late gastrula stage (Figure 4C). Similar to amphioxus, the *gsc* and *delta* expression domains overlapped on the ventral side of the embryos (Figures 4A, 4D, S6B, and S4C). The spotty distribution of *delta* seen in the overlying ectoderm of E1 and E2 likely corresponds to that observed in S1 and S2 of amphioxus (Figures 4A and 4D).<sup>28</sup> In *P. flava* embryos, not only *gsc* and *delta* but also expression domains of other homologs of vertebrate head mesodermal genes (*six3/6*, *otx1/2*, *tbx1/10*, *pitx2*) and somitogenesis-related genes (*hairy1*, *pax3/7*, *gbx1/2*, *six1/2*, *hox1*, *hox4*) were largely overlapped (Figure S7). These results suggest that this extant hemichordate has some developmental mechanisms of somitogenesis that are shared with amphioxus (Figure 4E). The enterocoel theory argues that somites evolved from trimeric coeloms (protocoel, mesocoel, and metacoel) of tornaria larvae.<sup>48</sup> However, current data and recent findings<sup>49</sup> suggest that somites are derived from the undifferentiated endomesoderm. Based on the similar genetic profiles between amphioxus and *P. flava* embryos, the mesoderm of the common ancestor of chordates is likely to have been an amphioxus-like unpolarized one.<sup>27,28</sup> Thus, the paraxial head mesoderm in vertebrates likely evolved via the reorganization of ancestral chordate mesodermal patterning.

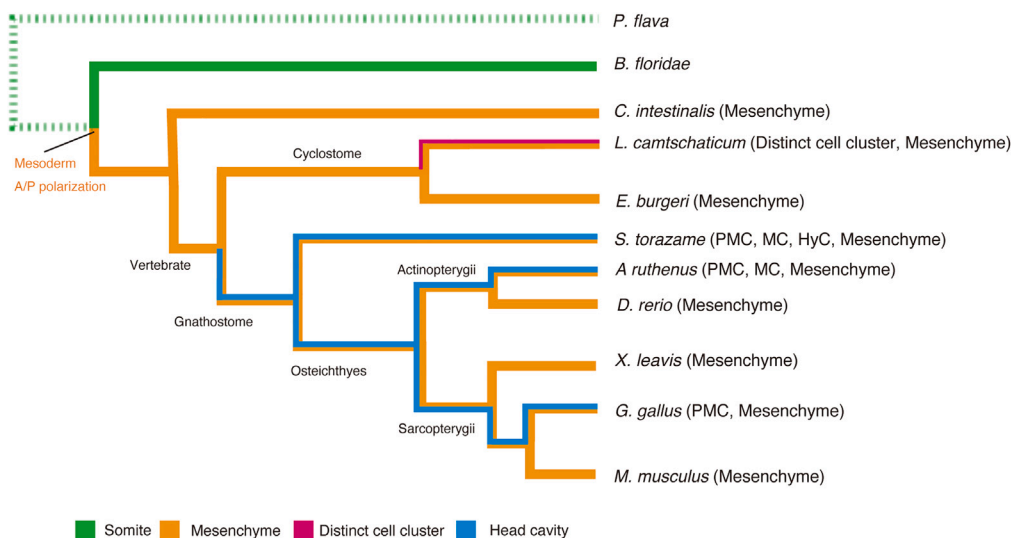


**Figure 5. Evolutionary scenario of the vertebrate head mesoderm**

See also Figures S7 and S8. A simple phylogeny of deuterostomes and evolution of the vertebrate head mesoderm. Dotted green line indicates that even hemichordate does not have somites; genetic profiles of the mesoderm is similar to amphioxus. The head mesoderm of tunicates includes a vertebrate cardiopharyngeal-like domain but not the paraxial domain. HyC, hyoid head cavity; MC, mandibular head cavity; PMC, premandibular head cavity.

## DISCUSSION

### Early diversification of the vertebrate craniofacial mesoderm

The key controversy regarding vertebrate head evolution is the presence/absence of somites in the pre-otic head mesoderm.<sup>2,4,5,24,25</sup> Our data indicated that the mandibular and hyoid cell clusters in the lamprey head mesoderm are not somite-like rosettes (Figure 2). The cell clusters are likely lamprey-specific features, which are organized by tightly situated amorphous and columnar cells with many spaces and are not recognized in the paraxial head mesoderm in hagfish and shark embryos.<sup>35,50</sup> Previous genetic and morphological studies on shark embryos indicated that head cavities are not homologous to somites.<sup>27,50</sup> The different organizations of the craniofacial mesoderm among lampreys (e.g., distinct mesenchymal cell clusters), hagfishes (mesenchyme), and gnathostomes (e.g., head cavities and mesenchyme) suggest that several variations of the unsegmented head mesoderm emerged during the initial diversification of vertebrate heads (Figure 5).<sup>5</sup> The presence of the mesenchymal head mesoderm, which includes cardiopharyngeal progenitors in tunicates, also supports this conclusion (Figure 5).<sup>51–53</sup> Emergence of mesenchymal cells in embryos might be crucial for the evolution of the vertebrate head. The neural crest (NC) is multipotent stem cells, and presence of the NC is a key for the evolution of the vertebrate head.<sup>54</sup> The migratory character of the NC cells (NCC), which first arises as epithelial cells in the ectoderm, enables to form new anatomical structures (e.g., jaws) in the head.<sup>6,54</sup> Current study indicates that acquisition of motility both in NCC and the head mesodermal cells is fundamental to the evolution of the vertebrate new heads.

### Rosettes and the head segmentation

Rosettes are major somite patterns. Therefore, historically, rosettes have been treated as a crucial characteristic of segments in the head problem. This concept expects somites to be equal to segments. However, the rosettes should be treated independently from segments.<sup>5</sup> For example, rosettes were found in the neural tube and during kidney formation (Figures S8Q and S8R).<sup>55</sup> These rosettes were not segments. Instead, these patterns arise frequently in organogenesis.<sup>55,56</sup> Recent studies using human iPS cells have shown that somite-like rosette patterns can be generated from presomitic mesoderm-like stem cells.<sup>57</sup> These rosettes recapitulated somitogenesis in embryos; however, their unique topological organization is never observed in the somitogenesis of wild-type vertebrate embryos.<sup>57</sup> This indicates that *in vitro*, the developmental environment for somite-like organoids is insufficient to set up somites as a row along the A/P axis.<sup>58</sup> Therefore, the self-organizing somite-like rosettes were not segments. These findings also support our perspective on rosettes as not segments, and mesodermal segments in embryos are defined as a row of cell blocks under proper spatiotemporal regulation during embryogenesis (Figures S8Q and S8R). Therefore, even if somite-like rosettes form in the head mesoderm of some vertebrate embryos, such evidence is not directly considered the presence of mesodermal segments in the head. How these rosettes evolved is unclear. During skin pattern formation in fish, fine-tuning the membrane potential of cells is essential for proper cell migration.<sup>59</sup> Ion channels are ancient genes that regulate cell motility in bacteria,<sup>60</sup> suggesting they are conserved for cell–cell communication. Consistent with this notion, the disruption of membrane potential by the over-expression of *kcn5b* (*W169L*) (a potassium channel) in zebrafish embryos resulted in the malformation of rosettes both in somites and Kupffer’s vesicles (an essential structure for left/right axial patterning)<sup>61</sup> (Figures S8A–S8P). Therefore, rosettes in different tissues may share mechanisms of cell motility, including signaling pathways that drive rosette formation.<sup>55</sup> In somitoids, regulation of cell motility is also reported

to be essential for rosette formation.<sup>57</sup> The diverse and conserved layers of the genetic system for rosette formation suggest that rosettes are robust embryonic tools essential for multiple steps in organogenesis. Future studies should investigate how rosettes participate in morphological individualization and whether they are developmental competences of morphological novelty that create new taxa via subsequent radiation.<sup>62</sup>

### Limitations of the study

3D reconstruction of the lamprey embryos by using dragonfly software technically needed lots of efforts, and we therefore performed one experiment for each stage. For SBF-SEM analysis, we have the same reason and performed the experiment once. Regarding the embryos obtained from the fields (e.g., amphioxus, shark), the samples were fixed and kept in our lab for several years (e.g., 10 years). This might have affected the quality of morphological and gene expression studies.

### STAR★METHODS

Detailed methods are provided in the online version of this paper and include the following:

- KEY RESOURCES TABLE
- RESOURCE AVAILABILITY
  - Lead contact
  - Materials availability
  - Data and code availability
- EXPERIMENTAL MODEL AND STUDY PARTICIPANT DETAILS
  - Animals
  - Lamprey
  - Shark
  - Chicken
  - Zebrafish
  - Amphioxus
  - Hemichordate
- METHOD DETAILS
  - Life science study design
  - Histological analysis
  - 3D reconstructions of lamprey embryos
  - Whole-mount *in situ* hybridization
  - Transmission electron microscopy (TEM) analysis
  - Toluidine blue staining
  - Serial block-face–scanning electron microscopy and 3D reconstruction using artificial intelligence
  - Zebrafish microinjection
  - Plasmid construction
  - Immunocytochemistry of zebrafish embryos
  - Phylogenetic tree analysis
- QUANTIFICATION AND STATISTICAL ANALYSIS

### SUPPLEMENTAL INFORMATION

Supplemental information can be found online at <https://doi.org/10.1016/j.isci.2023.108338>.

### ACKNOWLEDGMENTS

We thank Dr. R. Cerny of Charles University, Czech Republic, and Dr. N.D Holland of UCSD, USA, for the critical reading of the manuscript. We also thank Dr. L. Z. Holland of UCSD, USA, and Dr. P. W. H. Holland of the University of Oxford, UK, for the study discussion and Dr. S. Kuratani of RIKEN, Japan, for the discussion and the laboratory space. We thank Dr. H. Nagashima and N. Sato of Niigata University, Japan, for the collection of adult lamprey and suggestions for obtaining chicken eggs. We are grateful to Dr. S. Iino of the University of Fukui for supporting the project and Mr. Takagi of University of Fukui for providing technical help for TEM analysis. We also thank Dr. Yu and Dr. Su of Academia Sinica, Taiwan, for the discussion of data, embryos, and cDNA of *Ptychodera flava*. We thank A. Imai and N. Hattori (National Institute for Physiological Sciences) for their technical assistance. This work was supported by University of Fukui, Life Science Innovation Center, Japan, JSPS KAKENHI Grant-in-Aid for Scientific Research (C) 19K06787, JSPS KAKENHI Grant Number JP16H06280, Takeda Medical Foundation, and The Cooperative Study Programs of the National Institute for Physiological Sciences, Japan.

## AUTHOR CONTRIBUTIONS

Conceptualization: T.O., N.A.  
 Methodology: T.O., T.A., N.O., H.U., M.M.  
 Investigation: T.O., T.A., N.A., F.S., N.O., H.U., M.M.  
 Visualization: T.O., N.O., H.U., M.M.  
 Funding acquisition: T.O., F.S., N.O.  
 Writing—original draft: T.O., N.A., F.S.  
 Writing—review and editing: N.O., T.A., H.U.

## DECLARATION OF INTERESTS

The authors declare no competing financial interest.

## INCLUSION AND DIVERSITY

We support inclusive, diverse, and equitable conduct of research.

Received: July 25, 2023

Revised: September 20, 2023

Accepted: October 23, 2023

Published: November 13, 2023

## REFERENCES

- Goethe, J.W. (1790). Das Schädelgrüt aus sechs Wirbelknochen aufgebaut. . zur naturwissenschaft überhaupt, besonders zur morphologie. II 2 (cited in Gaupp 1898).
- Holland, L.Z., Holland, N.D., and Gilland, E. (2008). Amphioxus and the evolution of head segmentation. *Integr. Comp. Biol.* 48, 630–646. <https://doi.org/10.1093/icb/ict060>.
- Goodrich, E.S. (1930). *Studies on the Structure and Development of Vertebrates* (Macmillan).
- Neal, H.V., and Rand, H.W. (1936). *In Comparative Anatomy* (Philadelphia).
- Kuratani, S., and Adachi, N. (2016). What are Head Cavities? - A History of Studies on Vertebrate Head Segmentation. *Zoolog. Sci.* 33, 213–228. <https://doi.org/10.2108/zs150181>.
- Gans, C., and Northcutt, R.G. (1983). Neural crest and the origin of vertebrates: a new head. *Science* 220, 268–273.
- Gee, H. (2018). *Across the Bridge : Understanding the Origin of the Vertebrates* (The University of Chicago Press).
- Balfour, F.M. (1878). *A Monograph on the Development of Elasmobranch Fishes* (Macmillan).
- Koltzoff, N.K. (1902). Entwicklungsgeschichte des Kopfes von Petromyzon planeri; ein Beitrag zur Lehre über Metamerie des Wirbelthierkopfes. *Bulletin de la Societe Imperiale des Naturalistes de Moscou* 16, 259–589.
- Holland, L.Z., Kene, M., Williams, N.A., and Holland, N.D. (1997). Sequence and embryonic expression of the amphioxus engrailed gene (AmphiEn): the metamereric pattern of transcription resembles that of its segment-polarity homolog in *Drosophila*. *Development* 124, 1723–1732.
- Koop, D., Chen, J., Theodosiou, M., Carvalho, J.E., Alvarez, S., de Lera, A.R., Holland, L.Z., and Schubert, M. (2014). Roles of retinoic acid and Tbx1/10 in pharyngeal segmentation: amphioxus and the ancestral chordate condition. *EvoDevo* 5, 36. <https://doi.org/10.1186/2041-9139-5-36>.
- Meier, S. (1979). Development of the chick embryo mesoblast. Formation of the embryonic axis and establishment of the metamereric pattern. *Dev. Biol.* 73, 24–45.
- Martindale, M.Q., Meier, S., and Jacobson, A.G. (1987). Mesodermal metamerism in the teleost, *Oryzias latipes* (the medaka). *J. Morphol.* 193, 241–252.
- Gilland, E.H. (1992). Morphogenesis of Segmental Units in the Chordamesoderm and Neuroepithelium of *Squalus acanthias* (Harvard University). <https://www.webofscience.com/wos/pqdt/full-record/PQDT:64819376>.
- Tam, P.P., and Meier, S. (1982). The establishment of a somitomereric pattern in the mesoderm of the gastrulating mouse embryo. *Am. J. Anat.* 164, 209–225. <https://doi.org/10.1002/aja.1001640303>.
- Ordahl, C.P.e. (2000). Somitogenesis, part 1 and part 2. *Curr. Top. Dev. Biol.* 347, 311–388. 47 and 48, 1-316 in vol in vol. 348.
- Freund, R., Dörfler, D., Popp, W., and Wachtler, F. (1996). The metamereric pattern of the head mesoderm—does it exist? *Anat. Embryol.* 193, 73–80.
- Jouve, C., Imura, T., and Pourquie, O. (2002). Onset of the segmentation clock in the chick embryo: evidence for oscillations in the somite precursors in the primitive streak. *Development* 129, 1107–1117.
- Bothe, I., and Dietrich, S. (2006). The molecular setup of the avian head mesoderm and its implication for craniofacial myogenesis. *Dev. Dynam.* 235, 2845–2860. <https://doi.org/10.1002/dvdy.20903>.
- Froriep, A. (1892). *Entwicklungsgeschichte des Kopfes*. Anatomische Hefte; Zweite Abteilung. *Ergebnisse der Anatomie und Entwicklungsgeschichte* 1, 521–605.
- Kuratani, S. (1997). Spatial distribution of postotic crest cells defines the head/trunk interface of the vertebrate body: embryological interpretation of peripheral nerve morphology and evolution of the vertebrate head. *Anat. Embryol.* 195, 1–13.
- Kingsbury, B.F., and Adelman, H.B. (1924). The morphological plan of the head. *J. Cell Sci.* 52–68, 239–286.
- Onai, T. (2018). The evolutionary origin of chordate segmentation: revisiting the enterocoel theory. *Theory Biosci.* 137, 1–16. <https://doi.org/10.1007/s12064-018-0260-y>.
- Aldea, D., Subirana, L., Keime, C., Meister, L., Maeso, I., Marcellini, S., Gomez-Skarmeta, J.L., Bertrand, S., and Escriva, H. (2019). Genetic regulation of amphioxus somitogenesis informs the evolution of the vertebrate head mesoderm. *Nat. Ecol. Evol.* 3, 1233–1240. <https://doi.org/10.1038/s41559-019-0933-z>.
- Wang, H., Holland, P.W.H., and Takahashi, T. (2019). Gene profiling of head mesoderm in early zebrafish development: insights into the evolution of cranial mesoderm. *EvoDevo* 10, 14. <https://doi.org/10.1186/s13227-019-0128-3>.
- Northcutt, R.G. (1996). The origin of craniates: neural crest, neurogenic placodes, and homeobox genes. *Israel J. Zool.* 42, 273–313.
- Adachi, N., Takechi, M., Hirai, T., and Kuratani, S. (2012). Development of the head and trunk mesoderm in the dogfish, *Scyliorhinus torazame*. II. Comparison of gene expression between the head mesoderm and somites with reference to the origin of the vertebrate head. *Evol. Dev.* 14, 257–276. <https://doi.org/10.1111/j.1525-142X.2012.00543.x>.
- Onai, T., Aramaki, T., Inomata, H., Hirai, T., and Kuratani, S. (2015). Ancestral mesodermal reorganization and evolution of the vertebrate head. *Zoological Lett.* 1, 29. <https://doi.org/10.1186/s40851-015-0030-3>.
- Janvier, P. (2015). Facts and fancies about early fossil chordates and vertebrates. *Nature* 520, 483–489. <https://doi.org/10.1038/nature14437>.
- Dupret, V., Sanchez, S., Goujet, D., Tafforeau, P., and Ahlberg, P.E. (2014). A primitive placoderm sheds light on the origin of the jawed vertebrate face. *Nature* 507, 500–503. <https://doi.org/10.1038/nature12980>.

31. Tian, Q., Zhao, F., Zeng, H., Zhu, M., and Jiang, B. (2022). Ultrastructure reveals ancestral vertebrate pharyngeal skeleton in yunnanozoans. *Science* 377, 218–222. <https://doi.org/10.1126/science.abm2708>.
32. Docker, M.F., Hume, J.B., and Clemens, B.J. (2015). Introduction: a surfeit of lampreys. In *Lampreys: biology, conservation and control*, M.F. Docker, ed. (Springer), pp. 1–34.
33. Evans, T.M., Janvier, P., and Docker, M.F. (2018). The evolution of lamprey (Petromyzontida) life history and the origin of metamorphosis. *Rev. Fish Biol. Fish.* 28, 825–838.
34. Miyashita, T., Coates, M.I., Farrar, R., Larson, P., Manning, P.L., Wogelius, R.A., Edwards, N.P., Anné, J., Bergmann, U., Palmer, A.R., and Currie, P.J. (2019). Hagfish from the Cretaceous Tethys Sea and a reconciliation of the morphological-molecular conflict in early vertebrate phylogeny. *Proc. Natl. Acad. Sci. USA* 116, 2146–2151. <https://doi.org/10.1073/pnas.1814794116>.
35. Oisi, Y., Ota, K.G., Kuraku, S., Fujimoto, S., and Kuratani, S. (2013). Craniofacial development of hagfishes and the evolution of vertebrates. *Nature* 493, 175–180. <https://doi.org/10.1038/nature11794>.
36. Dean, B. (1899). On the embryology of *Bdellostoma stouti* (Gustav Fischer), pp. 221–276. + pl. XV–XXVI.
37. Martini, F.H. (1998). The ecology of hagfishes. In *The biology of hagfishes*, J.M. Jorgensen, J.P. Lomholt, R.E. Weber, and H. Malte, eds. (Springer), pp. 57–77.
38. Hatta, S. (1893). On the formation of the germinal layers in Petromyzon. *J. Coll. Sci. Imp. Univ. Japan* 5, 221–276.
39. Damas, H. (1944). Recherches sur le développement de *Lampetra fluviatilis* L. Contribution à l'étude de la Céphalogenèse des vertébrés. *Archives de Biologie, Liège et Paris* 55, 1–248. + pl. I–III.
40. Kuratani, S., Horigome, N., and Hirano, S. (1999). Developmental morphology of the head mesoderm and reevaluation of segmental theories of the vertebrate head: evidence from embryos of an agnathan vertebrate, *Lampetra japonica*. *Dev. Biol.* 210, 381–400.
41. Pourquié, O. (2011). Vertebrate segmentation: from cyclic gene networks to scoliosis. *Cell* 145, 650–663. <https://doi.org/10.1016/j.cell.2011.05.011>.
42. Chal, J., and Pourquié, O. (2009). Patterning and Differentiation of the Vertebrate Spine. *The Skeletal System* 53, 41–116. Cold Spring Harbor Laboratory Press.
43. Chal, J., Guillot, C., and Pourquié, O. (2017). PACP couples the segmentation clock to somite morphogenesis by regulating N-cadherin-dependent adhesion. *Development* 144, 664–676. <https://doi.org/10.1242/dev.143974>.
44. Christ, B., Huang, R., and Scaal, M. (2007). Amniote somite derivatives. *Dev. Dynam.* 236, 2382–2396. <https://doi.org/10.1002/dvdy.21189>.
45. Onai, T., Aramaki, T., Inomata, H., Hirai, T., and Kuratani, S. (2015). On the origin of vertebrate somites. *Zoological Lett.* 1, 33. <https://doi.org/10.1186/s40851-015-0033-0>.
46. Tahara, Y. (1988). Normal stages of development in the lamprey, *Lampetra reissneri* (Dybowski). *Zool. Sci.* 5, 109–118.
47. Boorman, C.J., and Shimeld, S.M. (2002). Cloning and expression of a Pitx homeobox gene from the lamprey, a jawless vertebrate. *Dev. Genes Evol.* 212, 349–353. <https://doi.org/10.1007/s00427-002-0249-9>.
48. Masterman, A.T. (1899). On the theory of archimeric segmentation and its bearing upon the phyletic classification of the coelomata. *Proc. R. Soc. Edinb.* 22, 270–310.
49. Onai, T. (2019). Canonical Wnt/beta-catenin and Notch signaling regulate animal/vegetal axial patterning in the cephalochordate amphioxus. *Evol. Dev.* 21, 31–43. <https://doi.org/10.1111/ede.12273>.
50. Adachi, N., and Kuratani, S. (2012). Development of head and trunk mesoderm in the dogfish, *Scyliorhinus torazame*: I. Embryology and morphology of the head cavities and related structures. *Evol. Dev.* 14, 234–256. <https://doi.org/10.1111/j.1525-142X.2012.00542.x>.
51. Diogo, R., Kelly, R.G., Christiaen, L., Levine, M., Ziermann, J.M., Molnar, J.L., Noden, D.M., and Tzahor, E. (2015). A new heart for a new head in vertebrate cardiopharyngeal evolution. *Nature* 520, 466–473. <https://doi.org/10.1038/nature14435>.
52. Passamanek, Y.J., and Di Gregorio, A. (2005). Ciona intestinalis: chordate development made simple. *Dev. Dyn.* 233, 1–19. <https://doi.org/10.1002/dvdy.20300>.
53. Davidson, B. (2007). Ciona intestinalis as a model for cardiac development. *Semin. Cell Dev. Biol.* 18, 16–26. <https://doi.org/10.1016/j.semcdb.2006.12.007>.
54. Green, S.A., Simoes-Costa, M., and Bronner, M.E. (2015). Evolution of vertebrates as viewed from the crest. *Nature* 520, 474–482. <https://doi.org/10.1038/nature14436>.
55. Harding, M.J., McGraw, H.F., and Nechiporuk, A. (2014). The roles and regulation of multicellular rosette structures during morphogenesis. *Development* 141, 2549–2558. <https://doi.org/10.1242/dev.101444>.
56. Christodoulou, N., Kyprianou, C., Weberling, A., Wang, R., Cui, G., Peng, G., Jing, N., and Zernicka-Goetz, M. (2018). Sequential formation and resolution of multiple rosettes drive embryo remodelling after implantation. *Nat. Cell Biol.* 20, 1278–1289. <https://doi.org/10.1038/s41556-018-0211-3>.
57. Miao, Y., Djeflal, Y., De Simone, A., Zhu, K., Lee, J.G., Lu, Z., Silberfeld, A., Rao, J., Tarazona, O.A., Mongera, A., et al. (2023). Reconstruction and deconstruction of human somitogenesis in vitro. *Nature* 614, 500–508. <https://doi.org/10.1038/s41586-022-05655-4>.
58. Wimsatt, W.C. (1986). Developmental constraints, generative entrenchment, and the innate acquired distinction. In *Integrating Scientific Disciplines*, W. Bechtel, ed. (Springer), pp. 185–208.
59. Inaba, M., Yamanaka, H., and Kondo, S. (2012). Pigment pattern formation by contact-dependent depolarization. *Science* 335, 677. <https://doi.org/10.1126/science.1212821>.
60. Majumdar, S., and Pal, S. (2017). Cross-species communication in bacterial world. *J. Cell Commun. Signal.* 11, 187–190. <https://doi.org/10.1007/s12079-017-0383-9>.
61. Aamar, E., and Dawid, I.B. (2010). Sox17 and chordin are required for formation of Kupffer's vesicle and left-right asymmetry determination in zebrafish. *Dev. Dynam.* 239, 2980–2988. <https://doi.org/10.1002/dvdy.22431>.
62. Erwin, D.H. (2021). A conceptual framework of evolutionary novelty and innovation. *Biol. Rev. Camb. Philos. Soc.* 96, 1–15. <https://doi.org/10.1111/brv.12643>.
63. Ballard, W.W., Mellinger, J., and Lechenault, H. (1993). A series of normal stages for development of *Scyliorhinus canicula*, the lesser spotted dogfish (Chondrichthyes: Scyliorhinidae). *J. Exp. Zool.* 267, 318–336.
64. Hamburger, V., and Hamilton, H.L. (1951). A series of normal stages in the development of the chick embryo. *J. Morphol.* 88, 49–92.
65. Westerfield, M. (2007). *The Zebrafish Book. A Guide for the Laboratory Use of Zebrafish* (Printed by the University of Oregon Press).
66. Holland, L.Z., and Onai, T. (2011). Analyses of gene function in amphioxus embryos by microinjection of mRNAs and morpholino oligonucleotides. *Methods Mol. Biol.* 770, 423–438. [https://doi.org/10.1007/978-1-61779-210-6\\_16](https://doi.org/10.1007/978-1-61779-210-6_16).
67. Su, Y.H., Chen, Y.C., Ting, H.C., Fan, T.P., Lin, C.Y., Wang, K.T., and Yu, J.K. (2019). BMP controls dorsoventral and neural patterning in indirect-developing hemichordates providing insight into a possible origin of chordates. *Proc. Natl. Acad. Sci. USA* 116, 12925–12932. <https://doi.org/10.1073/pnas.1901919116>.
68. Sugahara, F., Aota, S.i., Kuraku, S., Murakami, Y., Takio-Ogawa, Y., Hirano, S., and Kuratani, S. (2011). Involvement of Hedgehog and FGF signalling in the lamprey telencephalon: evolution of regionalization and dorsoventral patterning of the vertebrate forebrain. *Development* 138, 1217–1226. <https://doi.org/10.1242/dev.059360>.
69. Uchida, K., Murakami, Y., Kuraku, S., Hirano, S., and Kuratani, S. (2003). Development of the adenohipophysis in the lamprey: evolution of epigenetic patterning programs in organogenesis. *J. Exp. Zool. B Mol. Dev. Evol.* 300, 32–47. <https://doi.org/10.1002/jez.b.44>.
70. Cardona, A., Saalfeld, S., Schindelin, J., Arganda-Carreras, I., Preibisch, S., Longair, M., Tomancak, P., Hartenstein, V., and Douglas, R.J. (2012). TrakEM2 software for neural circuit reconstruction. *PLoS One* 7, e38011. <https://doi.org/10.1371/journal.pone.0038011>.
71. Urakubo, H., Bullmann, T., Kubota, Y., Oba, S., and Ishii, S. (2019). UNI-EM: An Environment for Deep Neural Network-Based Automated Segmentation of Neuronal Electron Microscopic Images. *Sci. Rep.* 9, 19413. <https://doi.org/10.1038/s41598-019-55431-0>.
72. Perathoner, S., Daane, J.M., Henrion, U., Seebohm, G., Higdon, C.W., Johnson, S.L., Nüsslein-Volhard, C., and Harris, M.P. (2014). Bioelectric signaling regulates size in zebrafish fins. *PLoS Genet.* 10, e1004080. <https://doi.org/10.1371/journal.pgen.1004080>.
73. Kumar, S., Stecher, G., and Tamura, K. (2016). MEGA7: Molecular Evolutionary Genetics Analysis version 7.0. *Mol. Biol. Evol.* 33, 1870–1874.

STAR★METHODS

KEY RESOURCES TABLE

REAGENT or RESOURCE	SOURCE	IDENTIFIER
<b>Antibodies</b>		
β-catenin	SIGMA	Cat# C2206; RRID: AB_476831
anti-rabbit IgG Alexafluor 488	Invitrogen	A11070
<b>Chemicals, peptides, and recombinant proteins</b>		
CM-Dil	Invitrogen	C7000
DAPI	SIGMA	D9542
CellMask™ Deep Red	Invitrogen	C10046
Quetol812	Nissin EM	Cat. No. 340
propylene oxide	TGI	E0016
toluidine blue	Waldeck	34314-92
Potassium ferrocyanide	Wako	161-03742
Osumium tetroxide	Nissin EM	Cat. No. 3020-3
Thiocarbohydrazide	Alfa Aesar	L01205
L-aspartic acid	SIGMA	A9256
<b>Critical commercial assays</b>		
mMESSAGE mMACHINE™ SP6 Transcription Kit	Invitrogen	AM1340
PrimeSTAR® GXL DNA Polymerase	TAKARA	R050A
TOPO Blunt-End for Subcloning	Thermo Fisher	K280020
<b>Deposited data</b>		
Lcnotch MK509804	NCBI website	<a href="https://www.ncbi.nlm.nih.gov/">https://www.ncbi.nlm.nih.gov/</a>
Lcmesp MK509806	NCBI website	<a href="https://www.ncbi.nlm.nih.gov/">https://www.ncbi.nlm.nih.gov/</a>
Lcfringe MK509805	NCBI website	<a href="https://www.ncbi.nlm.nih.gov/">https://www.ncbi.nlm.nih.gov/</a>
Lcwnt3 OL441365	NCBI website	<a href="https://www.ncbi.nlm.nih.gov/">https://www.ncbi.nlm.nih.gov/</a>
Lcwnt8 OL441366	NCBI website	<a href="https://www.ncbi.nlm.nih.gov/">https://www.ncbi.nlm.nih.gov/</a>
Lccyp26 OL441363	NCBI website	<a href="https://www.ncbi.nlm.nih.gov/">https://www.ncbi.nlm.nih.gov/</a>
Lcraldh2 OL441364	NCBI website	<a href="https://www.ncbi.nlm.nih.gov/">https://www.ncbi.nlm.nih.gov/</a>
Pfdelta MW626948	NCBI website	<a href="https://www.ncbi.nlm.nih.gov/">https://www.ncbi.nlm.nih.gov/</a>
Pfhairy1 OQ689070	NCBI website	<a href="https://www.ncbi.nlm.nih.gov/">https://www.ncbi.nlm.nih.gov/</a>
Pfpax3/7 OQ689068	NCBI website	<a href="https://www.ncbi.nlm.nih.gov/">https://www.ncbi.nlm.nih.gov/</a>
Pfgbx1/2 OQ689069	NCBI website	<a href="https://www.ncbi.nlm.nih.gov/">https://www.ncbi.nlm.nih.gov/</a>
Pfsix1/2 OQ689067	NCBI website	<a href="https://www.ncbi.nlm.nih.gov/">https://www.ncbi.nlm.nih.gov/</a>
Pfpitx2 OQ689072	NCBI website	<a href="https://www.ncbi.nlm.nih.gov/">https://www.ncbi.nlm.nih.gov/</a>
Pftbx1/10 OQ689071	NCBI website	<a href="https://www.ncbi.nlm.nih.gov/">https://www.ncbi.nlm.nih.gov/</a>
<b>Experimental models: Organisms/strains</b>		
Branchiostoma floridae	Tampa, Florida, USA	N/A
Lethenteron camtschaticum	Hokkaido, Japan, Niigata, Japan	N/A
Scyliorhinus torazame	Ibaraki, Japan	N/A
Ptycodera flava	Taiwan	N/A
Gallus gallus	Yamagishi internet store	<a href="http://yuseiran.cart.fc2.com/laws">http://yuseiran.cart.fc2.com/laws</a>
<b>Software and algorithms</b>		
ImageJ	ImageJ	V1.53e

(Continued on next page)

**Continued**

REAGENT or RESOURCE	SOURCE	IDENTIFIER
MEGA7	MEGA	<a href="https://www.megasoftware.net/">https://www.megasoftware.net/</a>
Dragonfly	Object Research System, Canada	Ver 4.1.0.647
Amira	FEL	N/A
Grapher	Golden Software	Ver20.1.251
UNI-EM	GitHub, Inc	<a href="https://github.com/">https://github.com/</a>

**RESOURCE AVAILABILITY**

**Lead contact**

Further information and requests for resources and reagents should be directed to and will be fulfilled by the lead contact, Takayuki Onai ([tonai@u-fukui.ac.jp](mailto:tonai@u-fukui.ac.jp)).

**Materials availability**

This study did not generate new unique reagents.

**Data and code availability**

- All DNA sequences used in this study are available in NCBI web and accession numbers are listed in the [key resources table](#). Microscopy data used in this study is also available from the [lead contact](#) upon request.
- This paper does not report original code.
- Any additional information required to reanalyze the data reported in this paper is available from the [lead contact](#) upon request.

**EXPERIMENTAL MODEL AND STUDY PARTICIPANT DETAILS**

**Animals**

The sexually mature males and females and embryos of all animals (See details information below) used in this study were collected and cultured under group housed condition in compliance with the guidelines of the University of Fukui Animal Care and Use Committee Program. For sampling embryos, we did not test whether the influence of sex on the results of the study is significant. On our research's generalizability, even we consider that sex does not affect our results since the collected embryos were early stages, this might cause some limitation. No statistical methods were used to pre-determine the appropriate sample size to the animals and embryos used in this study. Sample sizes were determined based on empirically reasonable numbers with considering the 3Rs (reduction/refinement/replacement). We randomly selected embryos to experimental groups. During culture, we excluded dead embryos or malformed embryos from the selections.

**Lamprey**

Sexually mature male and female lampreys (*Lethenteron camtschaticum*) were collected from Niigata and Hokkaido, Japan in March to May 2012–2022 and kept in flow through tanks filled with 10°C to 12°C aerated water without feeding. We checked the health of lampreys almost every day and if there were dead individuals, we excluded them from the tanks since dead individuals were toxic and affect the health of other living adults. *In vitro* fertilization was performed, and embryonic stages (neurula and pharyngeal stages) were assessed as previously described.<sup>46</sup>

**Shark**

Sexually mature male and female sharks (*Scyliorhinus torazame*) were sampled in Ibaraki, Japan, in October 2012 and housed in tanks filled adjusted around 16°C with artificial seawater in 2012–2017. Sharks were fed with seafood mix (e.g., squids) at least once a week. Their eggs were collected when we found them in the tanks and cultured in the same tanks until the appropriate stage was reached and were then collected, and embryonic stages (pharyngeal stages) were assessed as described previously.<sup>63</sup>

**Chicken**

Chicken (*Gallus gallus*) eggs were purchased from Yamagishi Academic Fertile Egg Internet Store, Mizusawa, Yokkaichi, Mie, Japan (<http://yuseiran.cart.fc2.com/laws>), and stored at 38°C incubator until the required stage (neurula to pharyngeal stages) was reached, with embryonic stages determined as described previously.<sup>64</sup>

**Zebrafish**

Sexually mature male and female zebrafish (*Danio rerio*) Tübingen strain were bred and maintained at 25°C under standard laboratory conditions in 2021.<sup>65</sup> Artificial spawning was performed following as previously described.<sup>65</sup> 1-cell stage fertilized eggs were collected for microinjection.

### Amphioxus

Sexually mature male and female amphioxus (*Branchiostoma floridae*) embryos were collected from Tampa Bay, Florida, USA, in July 2011, and brought to a laboratory at university of south Florida by evening. Around 21:00, electro-stimulation was performed to adult amphioxus (males and females) to induce spawning, and embryos (gastrula, neurula) were obtained via *in vitro* fertilization, with embryonic stages determined as previously described.<sup>66</sup>

### Hemichordate

Embryos (40 hours postfertilization) and larvae (70 hours postfertilization) of the hemichordate (*Ptychodera flava*) were kindly gifted by Dr. Yu and Dr. Su.

## METHOD DETAILS

### Life science study design

Some experiments such as TEM analysis and 3D reconstruction of embryos were performed once since hard to collect embryos or technical difficulty. For data exclusions, before fixation or before starting methods after fixation, we excluded dead embryos and larvae, therefore not counted. Embryos and larvae when failed *in situ* hybridizations, histological staining due to technical issues (e.g., degraded reagents) were not counted. To confirm the results, we mostly performed more than two times to confirm reproducibility except for some results (see above). For randomization, wild lamprey, *P. flava*, amphioxus and shark adults were chosen based on health and fertility. For 38 degrees incubation of chicken eggs, we selected eggs randomly. Embryos were selected randomly for histological staining, *in situ* hybridization. For Blinding, Blinding is not necessary since controls were performed in parallel for each experimental condition. Sample size determination was considered based on empirically reasonable numbers.

### Histological analysis

The collected lamprey, shark, and chicken embryos were fixed in 4% paraformaldehyde (PFA) in phosphate-buffered saline (PBS) and washed using a graded series of methanol. They were then placed in CM-Dil (Invitrogen, MA, USA) dissolved in 50  $\mu$ L BABB (1:2 mixture of benzyl alcohol/benzyl benzoate) for 1 h at room temperature. After washing twice with BABB, the embryos were optically sectioned using a laser scanning microscope (Zeiss LSM 710, Germany or Olympus FVI200, Japan).

Amphioxus and hemichordate embryos were placed in 4',6-diamidino-2-phenylindole (DAPI, Invitrogen, MA, USA) in PBS with Tween™ 20 (PBST) for 2 min and then in CellMask™ Deep Red (Invitrogen, MA, USA) in PBST for 20 min. They were washed three times in PBST, treated with 80% glycerol, and sectioned using a laser scanning microscope (Olympus FVI200, Japan).

Each image was rotated and cropped, following which brightness and contrast adjustments were made to the entire image using the Adobe Photoshop 2023 software (Adobe, CA, USA). Panels were then created using Adobe Illustrator 2023 and Dragonfly software (Object Research Systems, Montreal, Canada).

### 3D reconstructions of lamprey embryos

3D reconstructions of lamprey embryos (stages 17–26) were generated using the Dragonfly software (Ver. 4.1.0.647). For segmentation of each embryonic structure (e.g., somites), New region of interest (ROI) was created and round brush tool was chosen. Morphological structure of ROI was judged by images obtained by laser scanning microscope (Olympus FVI200, Japan) or upright microscope with camera (Olympus BX53, DP80, Japan). After segmented a target structure in all slices, each segment was connected and 3D view command was selected to confirm reconstruction of ROIs. After generation of 3D structure, Smooth Mesh tool was used to smoothen the structure. Usually, less than five times of smooth command was applied. To prepare samples, lamprey embryos were fixed in 4% PFA in PBS, and washed by graded series of methanol (50%–100%). Optical sections (2- $\mu$ m thick) of the embryos were obtained by performing CM-Dil labeling and laser scanning (Olympus FVI200, Japan) as indicated in the histological analysis section, whereas plastic sections (2- $\mu$ m thick) were obtained for stages 25 and 26. Embryos were sectioned several times at each stage.

### Whole-mount *in situ* hybridization

Whole-mount *in situ* hybridization of lamprey, amphioxus, or hemichordate embryos was performed following previously published protocols.<sup>28,67</sup> The probes for *Lcnotch* (MK509804), *Lcmesp* (MK509806), *Lcfringe* (MK509805), *Lcwnt3* (OL441365), *Lcwnt8* (OL441366), *Lccyp26* (OL441363), *Lcraldh2* (OL441364), and *Lcfgf8/17*<sup>68</sup> were cloned from the complementary DNA of *L. camtschaticum* embryos using primers based on TBLASTN obtained from in-house RNA sequencing data (Figure S6). The probe for *Lcdelta* (KF564639) and *Lcbrachyury* (AB501127) was generated from a TOPO cloning vector as previously described.<sup>28</sup> *LcpitxA*<sup>69</sup> was cloned into pCRII Topo vector and transcribed by SP6 RNA polymerase (2520, TKR, Shiga, JAPAN) to generate anti-sense probe. *Lcgsc* probe were generated by using *Lcgsc*-pCRblunt II Topo vector and transcribed to make anti-sense probe by T7 RNA polymerase (2540A, TKR, Shiga, JAPAN) as described previously.<sup>28</sup> For *P. flava* genes, the probe for *delta* (MW626948), *hairy1* (OQ689070), *pax3/7* (OQ689068), *gbx1/2* (OQ689069), *six1/2* (OQ689067), *hox1* (AY436753), *hox4* (AY436754), *pax1/9* (AB020763.1), *tbx1/10* (OQ689071) were cloned from cDNAs, and Dr. Yu and Dr. Su kindly gifted the *gsc* (QBZ28539.1), *otx1/2* (AB028220), *pitx2* (OQ689072), *six3/6* (KP133095) genes cloned in pGEM-T Easy vector. For amphioxus probes,

*Bfgsc* (AF281674) was generated from *Bfgsc*-pCRII Topo vector and *Bfdelta* (BW899056) was generated from *Bfdelta*-pCRII Topo vector by using SP6 RNA polymerase (2520, TKR, Shiga, JAPAN) as previously described.<sup>28</sup>

### Transmission electron microscopy (TEM) analysis

Lamprey embryos obtained in July 2016 were fixed in 2% PFA and 2.5% glutaraldehyde concentrate/PBS (–) for 2 h at room temperature and then stored at 4°C. The embryos were washed three times in 0.1 M phosphate (PB) buffer (pH 7.4) at room temperature. Re-fixed in 1% osmium tetroxide/0.1 M PB (pH 7.4) buffer at 4°C for 2 h in the dark. They were washed four times with 10% sucrose in water for 15 min each and block was stained with 2% uranyl acetate for 60 min at 4°C. Prior to sectioning, the samples were dehydrated using ethanol (50%, 70%, 90%, 95%, and 100%) serially, applying concentrations of 50%–95% ethanol for 10–15 min each, and 100% ethanol for 15 min four times. They were then treated twice with propylene oxide (PO) for 15 min each and subsequently placed in a 1:2 solution of epoxy resin (Quetol 812, Nissin EM, Japan):PO for 1 h at room temperature, a 2:1 solution of epoxy resin:PO overnight at room temperature, a 4:1 solution of epoxy resin:PO overnight at room temperature, and 100% epoxy resin twice for 2–3 h each at 37°C on rotation. The samples were then evacuated under 100% epoxy resin overnight at room temperature, after which they were embedded in epoxy resin at 60°C for 5–6 days. Ultrathin sections were produced using an ultramicrotome (Leica EM UC6, Japan) and double-stained with uranyl acetate and lead citrate. Images were obtained using an H-7650 electron microscope (Hitachi, Japan). The evacuation step was not performed for stage 25 lamprey embryos.

### Toluidine blue staining

Fixed lamprey embryos for TEM analysis were sectioned using an ultramicrotome (Leica EM UC6, Japan) to produce 2- $\mu$ m-thick sections. Toluidine blue solution [0.5% toluidine blue (Waldeck, Germany), 1% borax in water] was then added to the sections, and they were heated on a hot plate for 30 sec. The sections were washed with water and dried on a hot plate. Then the samples were covered by Entellan, and images were captured by upright microscope with camera (Olympus BX53, DP80, Japan).

### Serial block-face–scanning electron microscopy and 3D reconstruction using artificial intelligence

Embryos were fixed with 4% PFA, 2.5% glutaraldehyde concentrate/PBS (–), or 0.1 M PB at room temperature overnight. The embryos were then washed five times with PBS (–) or 0.1 M PB for 3 min. In total, 1.5% potassium ferrocyanide, 2% osmium tetroxide/PBS (–), or 0.1 M PB was added to the vials and rotated on ice for 1 h. The thiocarbonylhydrazide solution was added for 40 min at room temperature and washed four times with ultrapure water for 5 min. Two percent osmium tetroxide treatment for 30 min at room temperature was applied to the embryos, and they were washed four times for 5 min each using ultrapure water. Two percent uranyl acetate was added to the embryos and allowed to stand overnight at 4°C; these were washed five times using ultrapure water for 3 min. The modified bloc Walton's lead aspartate staining was performed for 30 min at 60°C; the embryos were then washed five times with ultrapure water for 3 min each and dehydrated using EtOH series from 50% to 100%. The samples were washed twice using PO for 15 min. The samples were then embedded in resin blocks, as described above. The samples in the resin blocks were trimmed and mounted on aluminum rivets with conductive glue (TK paste CR-2800, KAKEN TECH, Japan). The surfaces of the samples were trimmed, sputtered with gold to increase their conductivity, and imaged using a Merlin scanning electron microscope (Carl Zeiss Microscopy, Jena, Germany) equipped with a 3View in-chamber ultramicrotome (Gatan Inc., Pleasanton, CA, USA). The serial images were 16384  $\times$  16384 pixels wide (5–7 nm/pixel) at 50–70 nm steps in the depth direction. Serial images were processed and aligned using Fiji (<https://fiji.sc/>) with TrakEM2,<sup>70</sup> and segmentation and 3D reconstruction were performed using Amira (FEI, Hillsboro, OR, USA) and Dragonfly (Object Research Systems, Montreal, Canada). For nuclear segmentation, the training data were manually generated using Amira in the sub-volume of the EM images, used to train a convolutional neural network model, and yielded the inferred probability maps in UNI-EM version 0.90.4.<sup>71</sup> Probability maps were manually proofread using Amira.

### Zebrafish microinjection

The 1-cell stage eggs were collected and cultured at 25°C. Capped mRNAs generated by mMMESSAGE mMACHINE™ SP6 Transcription Kit (Thermo Fisher, MA, USA) were microinjected using a PV830 Pneumatic PicoPump (WPI). Injected embryos were developed at 28.5°C until the stages for analysis and collected based on a tracer expression (mCherryCx) located in the cell membrane.

### Plasmid construction

The tracer *mCherryCx* and gain-of-function mutant potassium channel *kcnk5b* (*W169L*)<sup>72</sup> Coding sequences (CDSs) were subcloned into a minimally modified pCS2 vector. Template plasmids were digested downstream of the polyA signal, and mRNAs were transcribed *in vitro* using the mMMESSAGE mMACHINE™ SP6 Transcription Kit (Thermo Fisher, MA, USA).

### Immunocytochemistry of zebrafish embryos

Embryos were fixed in 4% PFA/PBS for 2 h at room temperature. The embryos were dechorionated and washed thrice with PBS. Embryos were dissected using an ophthalmic knife to remove yolk granules and were separated into three regions (head/trunk/tail). Trunk tissues were used for studying somites, and tails were used to examine Kupffer's vesicles. The tissues were washed three times with PBS +0.1% triton for 20 min and blocked with PBS +0.1% triton, 10% sheep serum, and 0.5% bovine serum albumin solution for 2 h at room temperature. Either 1<sup>st</sup> antibody ( $\beta$ -catenin: SIGMA C2206) (SIGMA, MO, USA) or 2<sup>nd</sup> antibody (anti-rabbit IgG Alexafluor 488: Invitrogen A11070) (Invitrogen, MA, USA)

was added at a final concentration 1/400 for overnight at 4°C. The embryos were washed three times using PBS +0.1% triton for 20 min and counter-stained with DAPI (SIGMA, MO, USA). The samples were treated with 80% glycerol before observation by confocal microscopy (Olympus Fv1200, Japan).

### Phylogenetic tree analysis

Phylogenetic trees were constructed using the MEGA7 software.<sup>73</sup> Maximum likelihood analysis was performed using 1,000 bootstrap reiterations.

### QUANTIFICATION AND STATISTICAL ANALYSIS

Graphs were generated using the Grapher software (Golden Software, CO, USA).

The angles between AM-NP and AM-PM were calculated using the analysis command tool of Dragonfly, as follows: The regions of interest of the AM, NP, and PM were first converted into the locations of the center of mass. The vectors between the center points, that is,  $(x_{AM-NP}, y_{AM-NP}, z_{AM-NP})$  and  $(x_{AM-PM}, y_{AM-PM}, z_{AM-PM})$ , were then substituted into the inner product formula as follows:

$$\cos \theta = \frac{x_{AM-NP} * x_{AM-PM} + y_{AM-NP} * y_{AM-PM} + z_{AM-NP} * z_{AM-PM}}{\sqrt{x_{AM-NP}^2 + y_{AM-NP}^2 + z_{AM-NP}^2} \sqrt{x_{AM-PM}^2 + y_{AM-PM}^2 + z_{AM-PM}^2}}$$

Angle  $\theta$  was calculated and is displayed in Figure 1J, as demonstrated in Figure 1I that shows the transverse plane of their center points (blue: AM; green: NP; pink: PM).

The distances between the center points were also calculated and are displayed in Figures 1K and 1L:

$$\text{Distance V(AM-NP)} = \sqrt{x_{AM-NP}^2 + y_{AM-NP}^2 + z_{AM-NP}^2}$$

$$\text{Distance V(AM-PM)} = \sqrt{x_{AM-PM}^2 + y_{AM-PM}^2 + z_{AM-PM}^2}$$

The orientations of nuclei in the somites (Figure 2D) were analyzed in 2D space using the Dragonfly software. The angle was determined using a vector that connected the center of the rosette to the anterior–posterior (A/P) axis in the embryos, and the bar width was determined using Sturges’s formula:

$$K = \log_2 N + 1$$

Three individuals were examined for each cell cluster type (somite, mandibular arch cell cluster 1, cell cluster 2, and hyoid cell cluster) (Figures 2D–2G).

The angle of the head mesodermal cells was calculated by segmenting the paraxial head mesoderm at stage 20 in 2D space using Dragonfly software. A total of 28 column-like cells were selected as candidate somite-like cells. Cell nos. 1–6 were eliminated because they were in a single layer and, therefore, could not be considered somites. Cell nos. 7–28 were considered to have rosette organization if they were radially located. The center of the rosette was speculated to be in the middle along the dorsal/ventral axis (dotted line in Figure 2B). The angles of cell nos. 7–28 were calculated in 2D space using the Dragonfly software by drawing a vector along the A/P axis of the embryo (red arrow in Figure 2B) and a vector that extended from the cell (blue line in Figure 2B) to the red dotted line. The angle generated by these vectors was then calculated.

Embryos and structures were randomly selected in the experiments in this section. Sample size estimation was determined based on reasonable numbers for angle calculation. For inclusion and exclusion of data, dead embryos or malformed embryos were excluded before fixation.